ACS APPLIED MATERIALS & INTERFACES

Research Article

www.acsami.org

Sequential Deposition: Optimization of Solvent Swelling for High-Performance Polymer Solar Cells

Yao Liu,[†] Feng Liu,[†] Hsin-Wei Wang,[†] Dennis Nordlund,[‡] Zhiwei Sun,[†] Sunzida Ferdous,[†] and Thomas P. Russell*,[†]

[†]Department of Polymer Science & Engineering, Conte Center for Polymer Research, 120 Governors Drive, University of Massachusetts, Amherst, Massachusetts 01003, United States

[‡]Stanford Synchrotron Radiation Lightsource, SLAC National Accelerator Laboratory, Menlo Park, California 94025, United States

Supporting Information

ABSTRACT: Organic solar cells based on a typical DPP polymer were systematically optimized by a solvent swelling assisted sequential deposition process. We investigated the influence of solvent swelling on the morphology and structure order of the swollen film and the resultant device performance. Morphological and structural characterization confirmed the realization of ideal bulk heterojunctions using a suitable swelling solvent. A trilayered morphology was also found with the conjugated polymer concentrated bottom layer, $PC_{71}BM$ concentrated top layer, and interpenetrated networks of donor and acceptor in the middle by solvent swelling instead of thermal annealing in the sequential solution processing method. We proposed a simple strategy to optimize the sequential deposition fabricated devices by tuning the concentration of the $PC_{71}BM$ solution instead of thermal annealing. The best device showed a PCE of 7.59% with a V_{oc} of 0.61 V, J_{sc} of 17.95 mA/cm^2, and FF of 69.6%, which is the highest reported efficiency for devices fabricated by a sequential processing method and among the best results for DPP polymers.

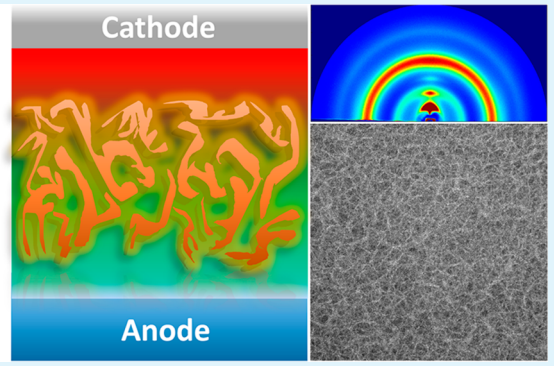

KEYWORDS: *conjugated polymer, solvent swelling, polymer solar cells, morphology characterization*

INTRODUCTION

Polymer solar cells (PSCs),[1−10] having the advantages of being cost effective, lightweight, and processable onto a flexible substrate by roll-to-roll printing techniques, have been the focus of much research.[11] The most efficient PSCs produced to date are mixed bulk heterojunction (BHJ) PSCs based on blends of conjugated polymers (donor) and fullerene derivatives (acceptor).[12−23] However, since the BHJ structure is kinetically trapped during solution processing,[24] balancing multiple kinetic processes to optimize crystallinity, domain size, orientation, and distribution of the components within the active layer is challenging.[25−31] The optimal BHJ morphologies must have efficient exciton dissociation and a balanced charge transport for electrons and holes to their respective electrodes.[32] Conventionally, PSCs are prepared by solution casting or spin coating a solution of mixed conjugated polymer and fullerene. Phase separation, ordering, and preferential segregation of components to either the lower electrode or the air interface dictate the morphology and performance. Kinetically trapped morphologies with characteristic length scales and interfacial segregation of the polymer and fullerene are realized that yield quite reasonable device efficiencies, though the morphology is certainly not optimized. The commonly used hole-transport buffer layer PEDOT:PSS has a high surface energy, and PCBM preferentially wets this interface, producing a nonfavorable gradient in the components.[33] Several groups have reported the fabrication of "bilayer" solar cells by casting a PCBM layer onto a polymer bottom layer to affect structures with a more suitable gradient of the donor and acceptor components.[34−46] Burn et al.[39] and Moulé et al.[41] showed neutron reflectometry plots for vertical concentration of their "bilayer" devices, demonstrating that the polymer swells with fullerene and that a fullerene-rich layer is left on top. Schwartz et al.[42] also showed how much fullerene goes into the polymer and that this can be controlled with the solvent choice in the sequential deposition. It is essential, though, to thermally anneal these bilayers to generate an interpenetrated morphology having performance comparable to conventional BHJs.[47−49] An alternate approach using such a bilayer strategy is to use the solvent in which the PCBM is dispersed to swell the initial polymer layer so as to enable penetration of the PCBM into the nonordered regions of the polymer. While avoiding the thermal annealing step, the favorable interactions of the PCBM with the solvent and the natural solvent gradient produced during solvent evaporation reduces the segregation of the PCBM to the anode interface and promotes segregation of

Received: October 7, 2014
Accepted: December 8, 2014
Published: December 8, 2014

Scheme 1. Procedures for SSA-SD Method and Molecular Structure of pDPP and $PC_{71}BM$

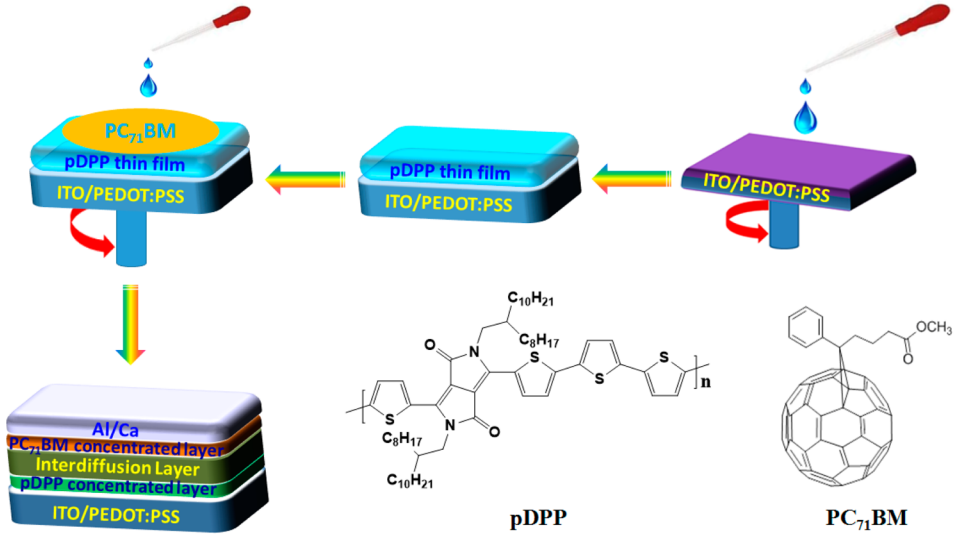

the PCBM to the surface onto which the cathode is placed. This process forces a vertically tiered morphology that is particularly well suited for OPV applications.

In this contribution, we use a solvent swelling assisted sequential deposition (SSA-SD) method to produce bulk heterojunction PSCs based on a crystalline diketopyrrolopyrrole (DPP) polymer (**pDPP**) and $PC_{71}BM$ (Scheme 1). Both the donor layer and the acceptor layer can be fabricated and optimized separately. Here, we fabricated devices in the forward geometry using **pDPP** as the bottom layer and $PC_{71}BM$ as the top layer. **pDPP** (Scheme 1) is a DPP-based conjugated polymer with high crystallinity and broad absorption of the solar spectrum[50] that is soluble in chloroform but can only be swollen by toluene (TOL), *o*-xylene (XY), chlorobenzene (CB), and 1, 2-dichlorobenzene (DCB).[50] Consequently, **pDPP** is an ideal material to probe the SSA-SD process and a good candidate to generate BHJ OPV devices. We find the property of the swelling solvent is critical for diffusion of $PC_{71}BM$ into the polymer layer. Table 1 shows the properties

Table 1. Solvent Properties: Boiling Point, Relative Polarity, and Hansen Solubility Parameters[51]

			Hansen solubility parameter		
solvent	bp (°C)	relative polarity	δ_D $[MPa]^{1/2}$	δ_P $[MPa]^{1/2}$	δ_H $[MPa]^{1/2}$
toluene	111	0.099	18.0	1.4	2.0
xylene	138	0.074	17.6	1.0	3.1
CB	131	0.188	19.0	4.3	2.0
DCB	181	0.225	19.2	6.3	3.3

of different solvents. Boiling points or vapor pressures of the swelling solvent have a significant influence on the final morphology of the swollen films. Morphology and structure characterization confirmed the realization of BHJs with a **pDPP** concentrated bottom layer, a $PC_{71}BM$ concentrated top layer, and interpenetrated networks of donor and acceptor in the middle by tuning the solvent swelling instead of thermal annealing in the sequential solution processing method. A systematic procedure was first proposed to optimize the SD-fabricated devices by tuning the concentration of the $PC_{71}BM$ solution. The best device fabricated using SSA-SD showed a PCE of 7.59% with a V_{oc} of 0.61 V, J_{sc} of 17.95 mA/cm^2, and FF of 69.6%, which, to our knowledge, is the highest reported efficiency for devices fabricated by a sequential processing method and also among the highest results for DPP polymers.

EXPERIMENTAL SECTION

Materials. $PC_{71}BM$ was obtained from Nano-C, Inc. Solvents used in this research were purchased from Sigma-Aldrich. **pDPP** was prepared by previously established procedures.[50] The molecular weight of the polymer was characterized with high-temperature GPC (Polymer Laboratories PL-220 with a refractive index detector) at 135 °C with 1,2,4-trichlorobenzene (Aldrich) as solvent. The results shown in Figure S1, Supporting Information, are based on calibration with polystyrene standards and yield M_n = 47 400, M_w = 84 600, PDI = 1.79.

Device Fabrication Procedure. The indium tin oxide (ITO)-coated glass substrates (20 ± 5 ohms/square) were bought from Thin Film Devices Inc. and cleaned through ultrasonic treatment in detergent, DI water, acetone, and isopropyl alcohol and then dried in an oven overnight. PEDOT:PSS (Clevios P VP AI 4083) (~35 nm) was spin coated onto ultraviolet ozone-treated ITO substrates. After annealing at 150 °C for 30 min in air, the substrates were transferred into a glovebox. The **pDPP** (5 mg/mL in chloroform: DCB = 4:1) was spin coated on top of the PEDOT:PSS layer at 1000 rpm. The thickness of the film was ~60−70 nm (KLA-TENCOR Alpha-Step IQ Surface Profiler). Then $PC_{71}BM$ dissolved in different solvents (toluene, *o*-xylene, chlorobenzene, and 1,2-dichlorobenzene) was drop casted onto the **pDPP** thin films. Allowing the $PC_{71}BM$ solution to swell and diffuse for about 60 s, we sequentially started spin- coating to form the "bilayer" structure with a thickness of ~80−100 nm. Finally, 15 nm calcium and then 100 nm Al cathode was deposited (area 6 mm^2 defined by metal shadow mask) on the active layer under high vacuum (2×10^{-4} Pa) using a thermal evaporator. All current−voltage (I−V) characteristics of the devices were measured under simulated AM1.5G irradiation (100 mW cm^{-2}) using a Xe lamp-based Newport 91160 300-W Solar Simulator. A Xe lamp equipped with an AM1.5G filter was used as the white light source. The light intensity was adjusted with an NREL-calibrated Si solar cell with a KG-5 filter. Photon mask was used during the measurement. The light exposure area (5.5 mm^2) of the devices was defined using a photomask with an aperture.

Characterization. Grazing incidence wide-angle X-ray diffraction (GIXD) characterization of the thin films was performed at the Stanford Synchrotron Radiation Lightsource (SSRL) on beamlines 11-3. The scattering intensity was recorded on a 2 D image plate (MAR-

dx.doi.org/10.1021/am506868g | ACS Appl. Mater. Interfaces 2015, 7, 653−661

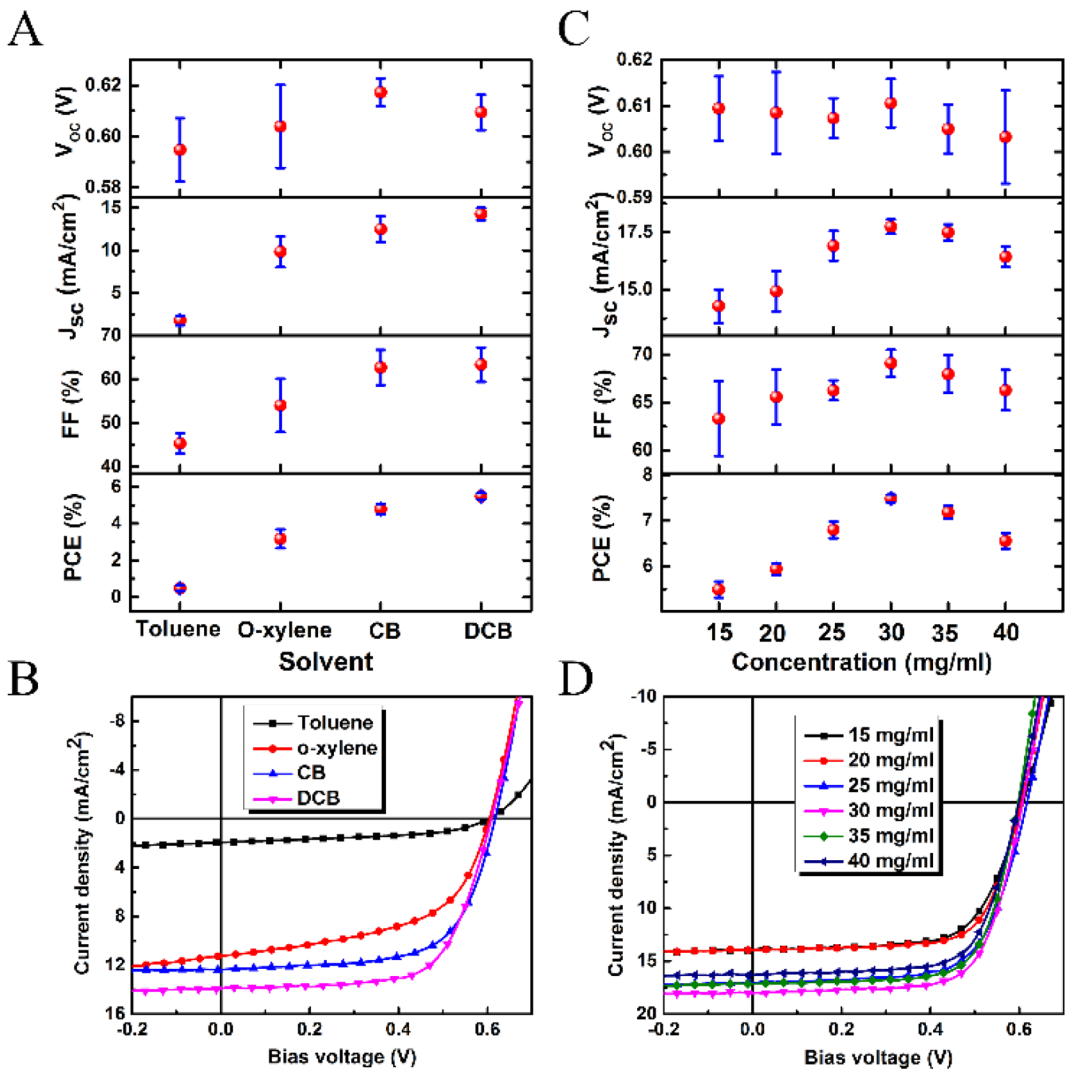

Figure 1. (A) Critical parameters of the device fabricated using toluene, *o*-xylene, CB, and DCB as swelling solvent ($PC_{71}BM$ solution concentration is 15 mg/mL), and the corresponding typical (B) *J*–*V* curve. (C) Critical parameters of the device fabricated using different concentrations of $PC_{71}BM$ solution in DCB, and the corresponding typical (D) *J*–*V* curve. (Parameters derived from at least 8 devices for each condition.)

345) with a pixel size of 150 μm (2300 × 2300 pixels). Samples were ~10 mm long in the direction of the beam path, and the detector was located at a distance of 400 mm from the sample center (distance calibrated using a Lanthanum hexaboride standard). The incidence angle was chosen in the range of 0.10–0.12° to optimize the signal-to-background ratio. The beam size was 50 μm × 150 μm, which resulted in a beam exposure on the sample 150 μm wide over the entire length of the 10 mm long sample. Data were distortion corrected (θ-dependent image distortion introduced by planar detector surface) before performing quantitative analysis on the images using the software WxDiff. The overall resolution in the GIXD experiments, dominated by the sample size, was about 0.01 Å^{-1}.

Resonant soft X-ray scattering (RSoXS) was measured at ALS beamline 11.0.1.2 using a transmission geometry. Samples were loaded on silicon nitride substrates, and the beam energy used was 284.4 eV, which generally probes the carbon edge resonance.[50]

Bright-field transmission electron microscopy (TEM) studies were conducted with a JEOL 2000 FX TEM operating at an accelerating voltage of 200 kV. Atomic force microscopy was performed on a Digital Instruments Dimension 3100, operating in tapping mode. To characterize the bottom surface of the thin film, we prepared samples according the procedures reported previously.[50]

X-ray photoelectron spectra (XPS) were recorded with a PerkinElmer-Physical Electronics 5100 with Mg KR excitation (400 W). Spectra were obtained at three different takeoff angles, 15°, 45°, and 75° (angle between the surface plane and the entrance lens of the detector optics). To characterize the bottom surface of the thin film, we prepared samples according the procedures we reported previously.[47]

RESULTS AND DISCUSSION

A thin film of **pDPP** was spin coated onto a PEDOT:PSS-coated ITO substrate (Scheme 1). $PC_{71}BM$, dissolved in orthogonal solvent, was drop cast onto the **pDPP** film (Scheme 1), allowing ~60 s for the **pDPP** to swell and the $PC_{71}BM$ to diffuse into the **pDPP**, then spin coated to evaporate the solvent. In this initial study we maintained a constant $PC_{71}BM$ solution concentration of 15 mg/mL. Toluene, *o*-xylene, chlorobenzene (CB), and 1,2-dichlorobenzene (DCB) were used to dissolve the $PC_{71}BM$, and the resultant device performances were compared (see Figure 1A and Table S1, Supporting Information). With increasing boiling point (or decreasing vapor pressure) of the solvent, a steady increase in the short circuit current (J_{sc}) and fill factor (FF) (Figure 1B) were observed, indicating a finer BHJ morphology. With DCB, a more polarized solvent with higher boiling point, more than a 7-fold improvement of the J_{sc} was observed, suggesting a greatly

dx.doi.org/10.1021/am506868g | ACS Appl. Mater. Interfaces 2015, 7, 653–661

improved BHJ morphology. While DCB is a poor solvent for **pDPP**,[51] the penetration of $PC_{71}BM$ into **pDPP** is evident. Consequently, DCB must swell the amorphous **pDPP**, and its lower vapor pressure translates into a longer residence time in the film, allowing the $PC_{71}BM$ to penetrate. It should also be noted that the device performance achieved by the SSA-SD process can even surpass BHJs fabricated by conventional spin coating of the blend solution (PCE ≈ 5.6%) (Table S3, Supporting Information), suggesting it is a more effective route to fabricate BHJ OPV devices.

Optimization of the concentration of $PC_{71}BM$ penetrating into the **pDPP** can be tuned by varying the concentration of $PC_{71}BM$ in DCB. In conventional DPP polymer-based OPV devices the weight fraction of PCBM is usually >0.5.[20,52] Figure 1C and 1D, Table S2, and Figure S2, Supporting Information, show that the device performance (J_{sc} and FF) improved almost linearly with the $PC_{71}BM$ concentration up to 30 mg/mL in DCB before the performance began to decrease (due, more than likely, to formation of a thick $PC_{71}BM$ on the surface). The best device fabricated using SSA-SD showed a PCE of 7.59% with a V_{oc} of 0.61 V, J_{sc} of 17.95 mA/cm^2, and FF of 69.6%, which, to our knowledge, is the highest reported efficiency for devices fabricated by a sequential processing method and also among the best results for DPP polymers. Remarkably, the performance significantly exceeded record values of conventional, spin-coated BHJ devices based on **pDPP**. It should be noted that a J_{sc} of 17.95 mA/cm^2 is among the highest values for low-band-gap conjugated polymers.[2,20,52−56]

The morphology of the thin films was characterized using various topological, structural, and chemical sensitive techniques. Shown in Figure 2 are transmission electron microscopy (TEM) images of SSA-SD-processed thin films using different solvents for the $PC_{71}BM$. Toluene led to $PC_{71}BM$ aggregates (>200 nm in size) residing on the surface of the **pDPP** (Figures 2A and S3, Supporting Information) and poor penetration of the $PC_{71}BM$ into the **pDPP**, which severely limited device performance (J_{sc} =1.76 mA/cm^2, FF = 45.23%, and PCE = 0.47% on average.). While *o*-xylene swelled the **pDPP** and enabled some penetration of $PC_{71}BM$ into the **pDPP**, resulting in an improvement in the J_{sc} (9.83 mA/cm^2), FF (53.98%), and PCE (3.17%), smaller aggregates of $PC_{71}BM$ were evident (Figure 2B). With CB as the solvent for $PC_{71}BM$, a uniform distribution of $PC_{71}BM$ was observed where the size of the $PC_{71}BM$ aggregates became much smaller than those found in toluene- and *o*-xylene-processed films (Figure 2C), and a marked increase of J_{sc} (12.48 mA/cm^2), FF (62.67%), and PCE (4.8%) was found. Using DCB as the solvent for $PC_{71}BM$, the average aggregates of $PC_{71}BM$ decreased further (Figure 2D) and increases in the J_{sc} (17.74 mA/cm^2), FF (69.1%), and PCE (7.48%) were observed. At high concentrations of the $PC_{71}BM$ in DCB the amount of $PC_{71}BM$ loading in the active layer using the swelling approach was greater than that attained by the conventional spin coating approach, as evidenced by the increase in absorption at 400−600 nm by UV−vis absorption (Figure S4, Supporting Information). In addition, a thin layer of $PC_{71}BM$ was deposited on the surface that acted as a hole blocking layer or electron transport layer at the cathode interface.[57]

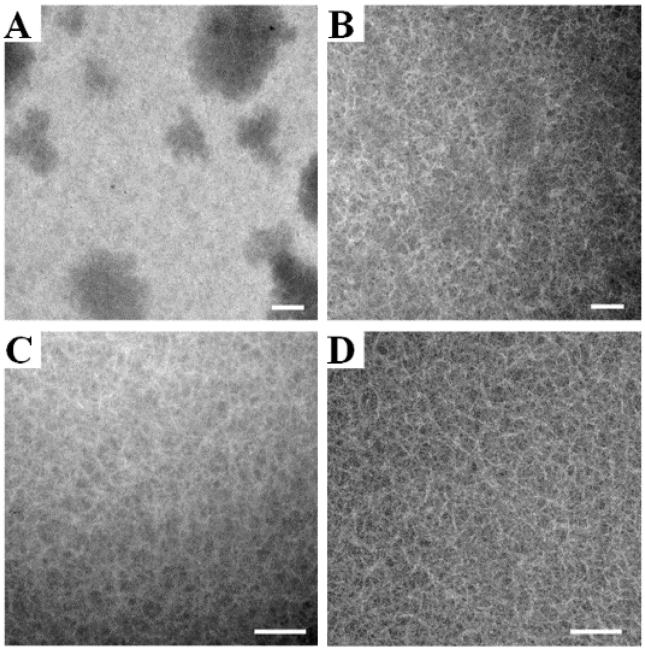

Figure 2. TEM morphology of thin films prepared with (A) toluene, (B) *o*-xylene, (C) chlorobenzene, and (D) dichlorobenzene as swelling solvent (scale bar is 200 nm).

Using atomic force microscopy (AFM), we found that the surface of the pure **pDPP** thin film was homogeneous with evidence for fibrillar structures (Figure 3A). The surface roughness increased when washing the films with DCB (Figure 3B). After spin coating a $PC_{71}BM$/DCB solution onto the **pDPP** film (Figure 3C), the surface was found to be smooth, suggesting that $PC_{71}BM$ or a mixture of $PC_{71}BM$ and amorphous **pDPP** is present after solvent evaporation. If this film was rinsed with toluene (a good solvent for $PC_{71}BM$ but poor solvent for **pDPP**) followed by drying, the remaining surface became even rougher, suggesting that some of the $PC_{71}BM$ that had diffused into the **pDPP** was also extracted (Figure 3D). The morphology at the bottom surface (near PEDOT:PSS) of the thin films was measured by removing the active layer from the PEDOT:PSS and transferring the active layer to a separate substrate with the original bottom interface facing upward. A rough bottom surface was observed for both a pure **pDPP** film and a DCB swelled **pDPP** film (Figure 3E and 3F). After swelling with $PC_{71}BM$/DCB solution (Figure 3G) and washing with toluene (Figure 3H), this bottom surface morphology of the film was also modified, indicating that $PC_{71}BM$ can diffuse through the entire polymer thin film, forming mixed BHJ structure to harvest photons, leading to an enhanced photocurrent.

Angle-dependent XPS was used to determine the elemental composition at the top few nanometers of the surface (Figure S5, Supporting Information). Table 2 summarizes the element composition (in atomic fractions) of the top surface and bottom surfaces of the thin film. Nitrogen (N 1s) and sulfur (S 2p) signals were used to label **pDPP**. We note that for a pure **pDPP** film the expected nitrogen and sulfur atomic fractions are ∼3% and ∼6%, respectively. For the top surface of the thin film (at a depth of 1−1.5 nm, 15° takeoff angle), both nitrogen and sulfur showed an atomic fraction of <1% (less than 30% **pDPP**). With increased detection depth (75° takeoff angle), the **pDPP** content increased (nitrogen and sulfur atomic fractions increased to ∼1%), confirming a gradient with more $PC_{71}BM$ on the top surface. Near-edge X-ray absorption spectroscopy (NEXAFS) displays a rich sensitivity to different functional

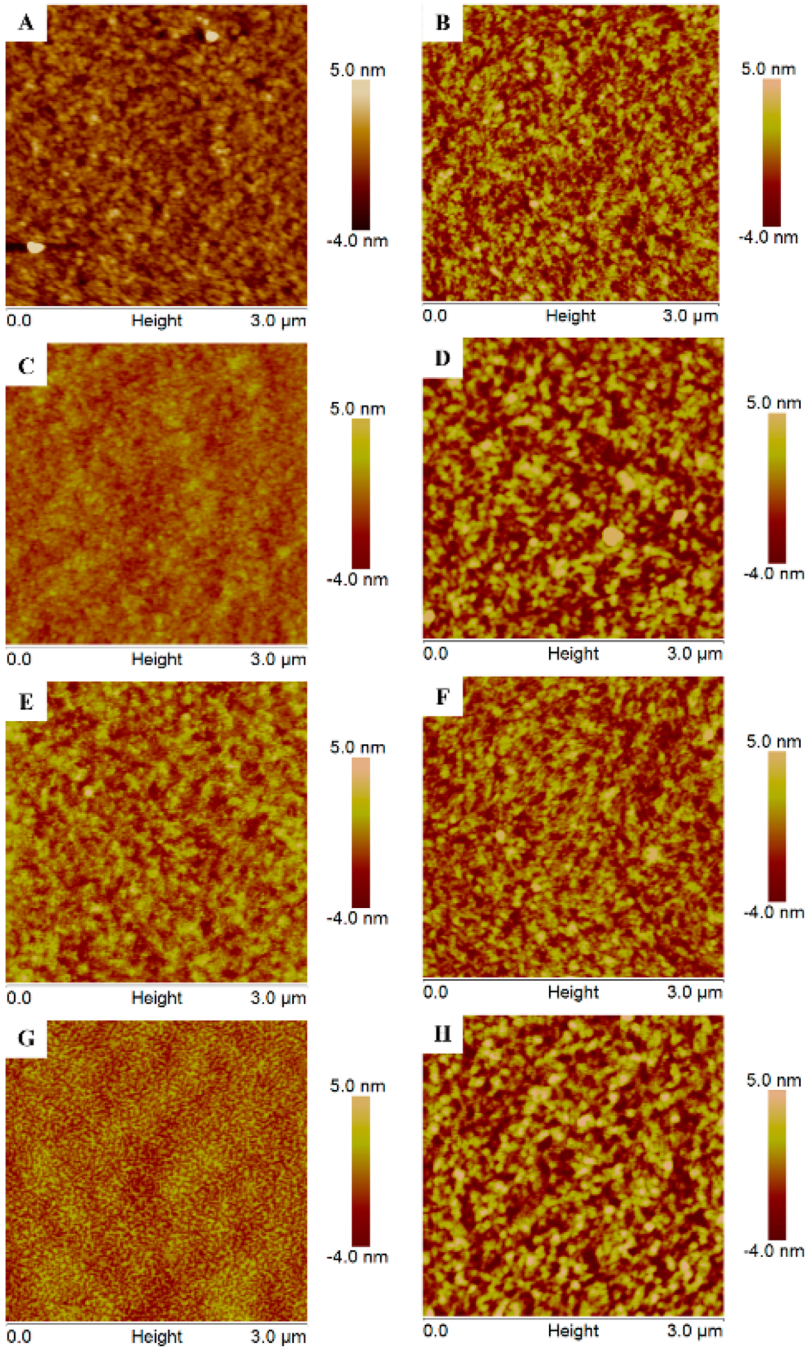

Figure 3. AFM topographic image for the top surface of (A) pure **pDPP** film, (B) pure **pDPP** film swelled by DCB, (C) blend film prepared by the SSA-SD process and then (D) after washing by toluene and the bottom surface of (E) pure **pDPP** film, (F) pure **pDPP** film swelled by DCB, and (G) blend film prepared by the SSA-SD process and then (H) after washing by toluene.

Table 2. Angle-Dependent XPS Provided Surface Element Composition of Thin Film Prepared by SSA-SD Process

		atom %			
surface	tilted angle (degrees)	S 2p	C 1s	N 1s	O 1s
top	15	0.9	87.4	0.6	11.1
	45	1.4	88.7	1.3	8.6
	75	1.3	90.0	1.0	7.6
bottom	15	6.1	87.3	3.6	2.9
	45	3.7	90.4	2.3	3.6
	75	3.3	91.9	1.7	3.0

groups and can be used to extract precise compositions for many blends in organic photovoltaics. We sampled the top ~5 nm of the surface by detecting NEXAFS in total electron yield (TEY) at the magic angle (to minimize angular effects). Through linear fitting of the spectrum we found that the top ~5 nm of the surface is composed of ~16% **pDPP** and ~84% $PC_{71}BM$ (Figure S6, Supporting Information), consistent with the XPS results. For the bottom surface of the thin film, XPS showed a nitrogen atomic fraction of 3.6%, which is close to the expected atomic fraction for a pure **pDPP** film. The nitrogen content decreased rapidly with increasing takeoff angle, demonstrating that $PC_{71}BM$ can diffuse fully through the

dx.doi.org/10.1021/am506868g | ACS Appl. Mater. Interfaces 2015, 7, 653−661

film. The vertical composition variation inside the bulk active layer was measured by dynamic secondary ion mass spectroscopy (DSIMS) using deuterated PCBM to label the location of the PCBM and S to locate the **pDPP** (Figure 4). The DSIMS

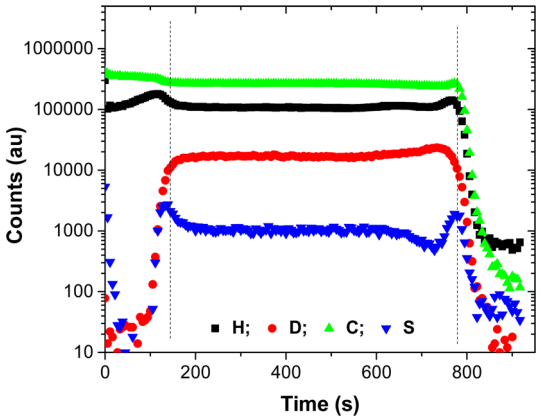

Figure 4. DISMS of thin film processed by SSA-SD.

profiles show the variation in the elemental composition of a sample as a function of sputtering time that corresponds to a depth in the film. For a uniform sample, quantitative conversion of sputtering time to depth requires a calibration of the sputtering rate of the pure components. However, with a phase-separated sample, differences in the sputtering rates of the components will give rise to broadening, making an absolute definition of the depth impossible. This is the case for our solvent swelling fabricated thin films, and as such, the profile was left as a function of the sputtering time. Since there is a gradient in the composition only over a few nanometers from the surface of the film, as evidenced by XPS, due to the resolution of DSIMS, we cannot determine the element composition quantitatively over this distance. The DSIMS results clearly point to a uniform distribution of components within the BHJ layer, which eliminates the possibility of a "pseudo bilayer" structure with gradients. AFM, XPS, NEXAFS, and DSIMS studies clearly demonstrated that SSA-SD processing leads to a sandwich structure with (1) a finely mixed BHJ layer in the middle, (2) a donor (**pDPP**) concentrated layer at the hole collecting electrode, and (3) an acceptor ($PC_{71}BM$) concentrated layer at the electron collecting electrode.

The structural order of the active layer prepared by SSA-SD processing was investigated by grazing incidence wide-angle X-ray diffraction (GIXD). Shown in Figure 5 are the GIXD patterns. All samples exhibited a sharp (100) reflection with up to four orders of reflections in the out-of-plane direction, indicating **pDPP** polymer adopt a well-defined edge-on orientation. The diffuse arc at ~1.4 $Å^{-1}$ in conjunction with less pronounced diffraction rings at ~2 $Å^{-1}$ arises from the $PC_{71}BM$. We did a line cut to get the out-of-plane (vertical cut) and in-plane (horizontal cut) scattering profiles (Figure 6). With a better swelling solvent, the diffraction peak location shifts to a lower q region, indicating an increased swelling degree of the polymer film. We find the $\pi-\pi$ stacking peak (010) is 1.6–1.7 $Å^{-1}$ in the in-plane scattering profile (Figure 6B), corresponding to a d spacing of 3.7 $Å^{-1}$. The (010) diffraction was suppressed with increasing penetration of $PC_{71}BM$ into the polymer film using a better swelling solvent, as evidenced by Figure 6B. Toluene is not a good solvent to swell the **pDPP** thin films, as evidenced by the similar UV–vis absorption profiles with and without swelling by pure toluene (Figure S7, Supporting Information). The inability of toluene to bring $PC_{71}BM$ into the polymer layer resulted in the $PC_{71}BM$ mostly depositing on top of the **pDPP** seen as grains in optical microscopy (Figure S3, Supporting Information). *o*-Xylene introduced $PC_{71}BM$ into the **pDPP** layer, slightly disturbed the packing of polymer chains and enhanced device performance. However, slight $PC_{71}BM$ aggregations can still be observed in the TEM image, indicating it is a marginal processing solvent (Figure 2B). More polarized solvents (chlorobenzene and dichlorobenzene) can swell the polymer layer well and effectively bring $PC_{71}BM$ into the polymer layer.

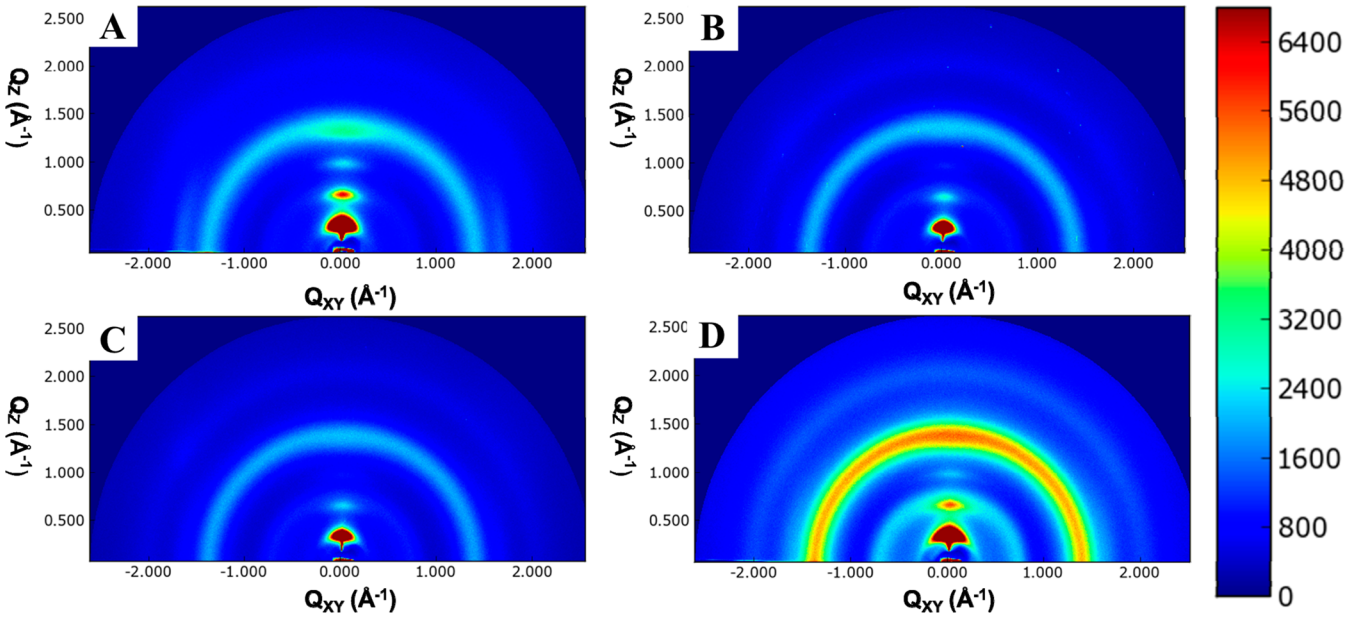

Figure 5. Two-dimensional GIXD patterns of the SSA-SD films fabricated using (A) toluene, (B) *o*-xylene, (C) CB, and (D) DCB as swelling solvent.

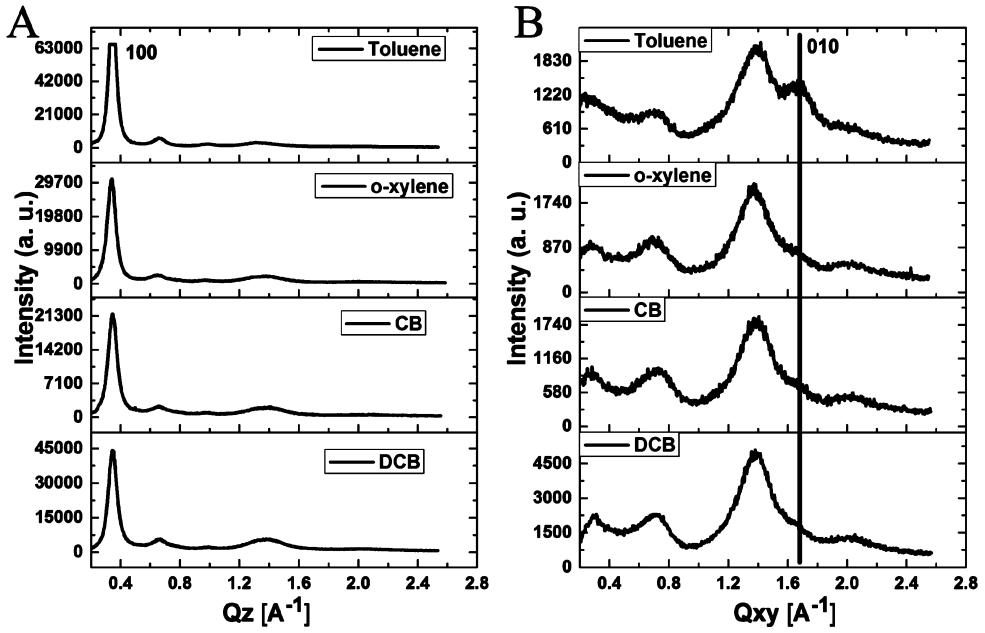

Figure 6. Corresponding (A) out-of-plane (vertical cut) and (B) in-plane (horizontal cut) scattering profiles of Figure 5.

The packing of the polymer is also affected. Since the diffusion of $PC_{71}BM$ was driven by the swelling process, the amount of $PC_{71}BM$ introduced into the polymer layer using non-halogenated solvents (toluene, *o*-xylene) is lower than that of halogenated solvents (CB, DCB), especially in the case of toluene (Figure S8, Supporting Information). RSoXS[30] offers better contrast between the active layer components at X-ray energies near the absorption edge and, due to the longer X-ray wavelength, access to a longer length scale. At an X-ray energy of 284.2 eV, the carbon K-edge, scattering contrast between the constituent moieties of **pDPP** polymer and the $PC_{71}BM$ was used in the transmission mode. RSoXS profiles (Figure 7) show a diffuse shoulder, corresponding to a domain size of ~64.0, ~48.8, and ~28.7 nm for the *o*-xylene, CB, and DCB swollen (and dried) films, respectively, which is consistent with the real space image provided by TEM. The sample swollen with toluene showed no obvious phase separation due to the lack of penetration of $PC_{71}BM$ into the **pDPP** (Figure S3, Supporting Information). These combined results clearly demonstrate that the swelling/interdiffusion is a viable route to generate BHJ OPV morphologies that is comparable to that generated by a conventional spin-coating method.

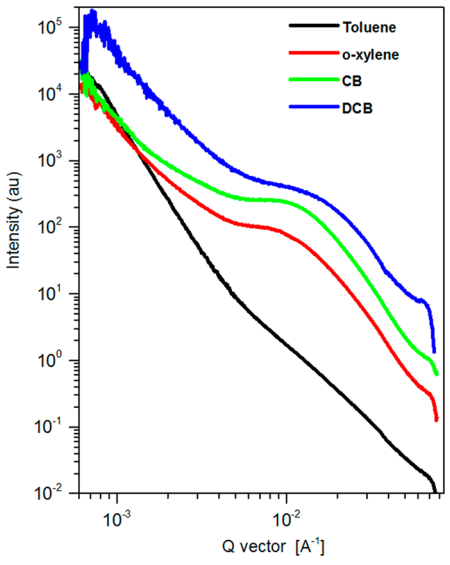

Figure 7. RSoXS profiles of the SSA-SD films fabricated using toluene, *o*-xylene, CB, and DCB as swelling solvent.

CONCLUSIONS

We successfully fabricated high-performance polymer solar cells by the SSA-SD process without using thermal annealing. A systematic device optimization was performed by varying the casting and diffusion conditions of the $PC_{71}BM$. PCEs of 7.59% were achieved. We investigated the influence of solvent properties (polarity and boiling point) on the morphology and structure order of the swollen film and the resultant device performance. Exploration of the device optimization procedure in the SD process was performed to further promote the development of this method. The nature of the fabrication generates a sandwich structure that is ideally suited for device applications. In addition, the ordered morphologies of the **pDPP** layer were preserved during the swelling process, leaving a very desirable continuous phase separated BHJ morphology. These results also suggest that morphology improvements can be achieved by optimizing the morphology of the **pDPP** initially, prior to the interdiffusion of the $PC_{71}BM$. Our SSA-SD processing strategy avoids using a postannealing procedure, taking full advantage of the natural solvent gradient produced during solvent evaporation, is a true solvent swelling process, and further development to sequential deposition. Consequently, the SSA-SD processing strategy is promising in generating highly efficient PSCs.

ASSOCIATED CONTENT

Supporting Information

Device performace, UV−vis absorption data, optical microscopy picture, X-ray photoelectron spectroscopy (XPS) profiles, NEXAFS profiles. This material is available free of charge via the Internet at http://pubs.acs.org.

dx.doi.org/10.1021/am506868g | ACS Appl. Mater. Interfaces 2015, 7, 653−661

AUTHOR INFORMATION

Corresponding Author

*E-mail: russell@mail.pse.umass.edu.

Notes

The authors declare no competing financial interest.

ACKNOWLEDGMENTS

This work was supported by the Department of Energy-supported Energy Frontier Research Center at the University of Massachusetts (DE-SC0001087). Portions of this research were carried out at beamline 11.0.1.2, 7.3.3 at the Advanced Light Source, Lawrence Berkeley National Laboratory, which was supported by the DOE, Office of Science, and Office of Basic Energy Sciences. Portions of this research were carried out at the Stanford Synchrotron Radiation Light Source, a national user facility operated by Stanford University on behalf of the U.S. Department of Energy, Office of Basic Energy Sciences under Contract No. DE-AC02-76SF00515. The authors thank Mr. Jacob Hirsch for assistance with XPS characterization.

REFERENCES

(1) Dou, L.; You, J.; Hong, Z.; Xu, Z.; Li, G.; Street, R. A.; Yang, Y. 25th Anniversary Article: A Decade of Organic/Polymeric Photovoltaic Research. *Adv. Mater.* **2013**, *25*, 6642−6671.

(2) Guo, X. G.; Zhou, N. J.; Lou, S. J.; Smith, J.; Tice, D. B.; Hennek, J. W.; Ortiz, R. P.; Navarrete, J. T. L.; Li, S. Y.; Strzalka, J.; Chen, L. X.; Chang, R. P. H.; Facchetti, A.; Marks, T. J. Polymer Solar Cells with Enhanced Fill Factors. *Nat. Photonics* **2013**, *7*, 825−833.

(3) Osaka, I.; Shimawaki, M.; Mori, H.; Doi, I.; Miyazaki, E.; Koganezawa, T.; Takimiya, K. Synthesis, Characterization, and Transistor and Solar Cell Applications of a Naphthobisthiadiazole-Based Semiconducting Polymer. *J. Am. Chem. Soc.* **2012**, *134*, 3498−3507.

(4) He, Z.; Zhong, C.; Su, S.; Xu, M.; Wu, H.; Cao, Y. Enhanced Power-Conversion Efficiency in Polymer Solar Cells Using an Inverted Device Structure. *Nat. Photonics* **2012**, *6*, 591−595.

(5) Liang, Y.; Xu, Z.; Xia, J.; Tsai, S.-T.; Wu, Y.; Li, G.; Ray, C.; Yu, L. For the Bright Future—Bulk Heterojunction Polymer Solar Cells with Power Conversion Efficiency of 7.4%. *Adv. Mater.* **2010**, *22*, E135−E138.

(6) Chen, H. Y.; Hou, J. H.; Zhang, S. Q.; Liang, Y. Y.; Yang, G. W.; Yang, Y.; Yu, L. P.; Wu, Y.; Li, G. Polymer Solar Cells with Enhanced Open-circuit Voltage and Efficiency. *Nat. Photonics* **2009**, *3*, 649−653.

(7) Li, G.; Shrotriya, V.; Huang, J.; Yao, Y.; Moriarty, T.; Emery, K.; Yang, Y. High-Efficiency Solution Processable Polymer Photovoltaic Cells by Self-organization of Polymer Blends. *Nat. Mater.* **2005**, *4*, 864−868.

(8) Yu, G.; Gao, J.; Hummelen, J. C.; Wudl, F.; Heeger, A. J. Polymer Photovoltaic Cells: Enhanced Efficiencies via a Network of Internal Donor-Acceptor Heterojunctions. *Science* **1995**, *270*, 1789−1791.

(9) Shrotriya, V.; Li, G.; Yao, Y.; Moriarty, T.; Emery, K.; Yang, Y. Accurate Measurement and Characterization of Organic Solar Cells. *Adv. Funct. Mater.* **2006**, *16*, 2016−2023.

(10) He, Z.; Zhong, C.; Huang, X.; Wong, W.-Y.; Wu, H.; Chen, L.; Su, S.; Cao, Y. Simultaneous Enhancement of Short-Circuit Current Density, and Fill Factor in Polymer Solar Cells. *Adv. Mater.* **2011**, *23*, 4636−4643.

(11) Sondergaard, R.; Hosel, M.; Angmo, D.; Larsen-Olsen, T. T.; Krebs, F. C. Roll-to-Roll Fabrication of Polymer Solar Cells. *Mater. Today* **2012**, *15*, 36−49.

(12) Cabanetos, C.; El Labban, A.; Bartelt, J. A.; Douglas, J. D.; Mateker, W. R.; Fréchet, J. M. J.; McGehee, M. D.; Beaujuge, P. M. Linear Side Chains in Benzo[1,2-b:4,5-b′]dithiophene−Thieno[3,4-c]pyrrole-4,6-dione Polymers Direct Self-Assembly and Solar Cell Performance. *J. Am. Chem. Soc.* **2013**, *135*, 4656−4659.

(13) Deng, Y.; Liu, J.; Wang, J.; Liu, L.; Li, W.; Tian, H.; Zhang, X.; Xie, Z.; Geng, Y.; Wang, F. Dithienocarbazole and Isoindigo Based Amorphous Low Bandgap Conjugated Polymers for Efficient Polymer Solar Cells. *Adv. Mater.* **2014**, *26*, 471−476.

(14) Thompson, B. C.; Fréchet, J. M. J. Polymer−Fullerene Composite Solar Cells. *Angew. Chem., Int. Ed.* **2008**, *47*, 58−77.

(15) Brabec, C. J.; Gowrisanker, S.; Halls, J. J. M.; Laird, D.; Jia, S.; Williams, S. P. Polymer−Fullerene Bulk-Heterojunction Solar Cells. *Adv. Mater.* **2010**, *22*, 3839−3856.

(16) Zhang, M.; Gu, Y.; Guo, X.; Liu, F.; Zhang, S.; Huo, L.; Russell, T. P.; Hou, J. Efficient Polymer Solar Cells Based on Benzothiadiazole and Alkylphenyl Substituted Benzodithiophene with a Power Conversion Efficiency over 8%. *Adv. Mater.* **2013**, *25*, 4944−4949.

(17) Zhang, M.; Guo, X.; Zhang, S.; Hou, J. Synergistic Effect of Fluorination on Molecular Energy Level Modulation in Highly Efficient Photovoltaic Polymers. *Adv. Mater.* **2014**, *26*, 1118−1123.

(18) Meager, I.; Ashraf, R. S.; Mollinger, S.; Schroeder, B. C.; Bronstein, H.; Beatrup, D.; Vezie, M. S.; Kirchartz, T.; Salleo, A.; Nelson, J.; McCulloch, I. Photocurrent Enhancement from Diketopyrrolopyrrole Polymer Solar Cells through Alkyl-chain Branching Point Manipulation. *J. Am. Chem. Soc.* **2013**, *135*, 11537−11540.

(19) Osaka, I.; Kakara, T.; Takemura, N.; Koganezawa, T.; Takimiya, K. Naphthodithiophene−Naphthobisthiadiazole Copolymers for Solar Cells: Alkylation Drives the Polymer Backbone Flat and Promotes Efficiency. *J. Am. Chem. Soc.* **2013**, *135*, 8834−8837.

(20) Hendriks, K. H.; Heintges, G. H. L.; Gevaerts, V. S.; Wienk, M. M.; Janssen, R. A. J. High-Molecular-Weight Regular Alternating Diketopyrrolopyrrole-based Terpolymers for Efficient Organic Solar Cells. *Angew. Chem., Int. Ed.* **2013**, *52*, 8341−8344.

(21) Li, K.; Li, Z.; Feng, K.; Xu, X.; Wang, L.; Peng, Q. Development of Large Band-Gap Conjugated Copolymers for Efficient Regular Single and Tandem Organic Solar Cells. *J. Am. Chem. Soc.* **2013**, *135*, 13549−13557.

(22) Li, W.; Yang, L.; Tumbleston, J. R.; Yan, L.; Ade, H.; You, W. Controlling Molecular Weight of a High Efficiency Donor-Acceptor Conjugated Polymer and Understanding Its Significant Impact on Photovoltaic Properties. *Adv. Mater.* **2014**, *26*, 4456−4462.

(23) Chen, Z.; Cai, P.; Chen, J.; Liu, X.; Zhang, L.; Lan, L.; Peng, J.; Ma, Y.; Cao, Y. Low Band-Gap Conjugated Polymers with Strong Interchain Aggregation and Very High Hole Mobility Towards Highly Efficient Thick-Film Polymer Solar Cells. *Adv. Mater.* **2014**, *26*, 2586−2591.

(24) Peet, J.; Senatore, M. L.; Heeger, A. J.; Bazan, G. C. The Role of Processing in the Fabrication and Optimization of Plastic Solar Cells. *Adv. Mater.* **2009**, *21*, 1521−1527.

(25) Ma, W.; Tumbleston, J. R.; Ye, L.; Wang, C.; Hou, J.; Ade, H. Quantification of Nano- and Mesoscale Phase Separation and Relation to Donor and Acceptor Quantum Efficiency, J_{sc}, and FF in Polymer:Fullerene Solar Cells. *Adv. Mater.* **2014**, *26*, 4234−4241.

(26) Kouijzer, S.; Michels, J. J.; van den Berg, M.; Gevaerts, V. S.; Turbiez, M.; Wienk, M. M.; Janssen, R. A. J. Predicting Morphologies of Solution Processed Polymer:Fullerene Blends. *J. Am. Chem. Soc.* **2013**, *135*, 12057−12067.

(27) Liu, F.; Wang, C.; Baral, J. K.; Zhang, L.; Watkins, J. J.; Briseno, A. L.; Russell, T. P. Relating Chemical Structure to Device Performance via Morphology Control in Diketopyrrolopyrrole-Based Low Band Gap Polymers. *J. Am. Chem. Soc.* **2013**, *135*, 19248−19259.

(28) Xiao, Z.; Yuan, Y.; Yang, B.; Vanderslice, J.; Chen, J.; Dyck, O.; Duscher, G.; Huang, J. Universal Formation of Compositionally Graded Bulk Heterojunction for Efficiency Enhancement in Organic Photovoltaics. *Adv. Mater.* **2014**, *26*, 3068−3075.

(29) Brabec, C. J.; Heeney, M.; McCulloch, I.; Nelson, J. Influence of Blend Microstructure on Bulk Heterojunction Organic Photovoltaic Performance. *Chem. Soc. Rev.* **2011**, *40*, 1185−1199.

(30) Liu, F.; Gu, Y.; Shen, X.; Ferdous, S.; Wang, H.-W.; Russell, T. P. Characterization of the Morphology of Solution-Processed Bulk Heterojunction Organic Photovoltaics. *Prog. Polym. Sci.* **2013**, *38*, 1990−2052.

(31) Liu, F.; Zhao, W.; Tumbleston, J. R.; Wang, C.; Gu, Y.; Wang, D.; Briseno, A. L.; Ade, H.; Russell, T. P. Understanding the Morphology of PTB7:PCBM Blends in Organic Photovoltaics. *Adv. Energy Mater.* **2014**, *4*, 1301377.
(32) Janssen, R. A.; Nelson, J. Factors Limiting Device Efficiency in Organic Photovoltaics. *Adv. Mater.* **2013**, *25*, 1847−1858.
(33) Germack, D. S.; Chan, C. K.; Kline, R. J.; Fischer, D. A.; Gundlach, D. J.; Toney, M. F.; Richter, L. J.; DeLongchamp, D. M. Interfacial Segregation in Polymer/Fullerene Blend Films for Photovoltaic Devices. *Macromolecules.* **2010**, *43*, 3828−3836.
(34) Ayzner, A. L.; Tassone, C. J.; Tolbert, S. H.; Schwartz, B. J. Reappraising the Need for Bulk Heterojunctions in Polymer-Fullerene Photovoltaics: The Role of Carrier Transport in All-Solution-Processed P3HT/PCBM Bilayer Solar Cells. *J. Phys. Chem. C* **2009**, *113*, 20050−20060.
(35) Li, H.; Qi, Z.; Wang, J. Layer-by-Layer Processed Polymer Solar Cells with Self-Assembled Electron Buffer Layer. *Appl. Phys. Lett.* **2013**, *102*, 213901−213903.
(36) Cheng, P.; Hou, J.; Li, Y.; Zhan, X. Layer-by-Layer Solution-Processed Low-Bandgap Polymer-PC61BM Solar Cells with High Efficiency. *Adv. Energy Mater.* **2014**, *4*, 1301349.
(37) Kim, D. H.; Mei, J.; Ayzner, A. L.; Schmidt, K.; Giri, G.; Appleton, A. L.; Toney, M. F.; Bao, Z. Sequentially Solution-Processed, Nanostructured Polymer Photovoltaics using Selective Solvents. *Energy Environ. Sci.* **2014**, *7*, 1103−1109.
(38) Wang, D. H.; Moon, J. S.; Seifter, J.; Jo, J.; Park, J. H.; Park, O. O.; Heeger, A. J. Sequential Processing: Control of Nanomorphology in Bulk Heterojunction Solar Cells. *Nano Lett.* **2011**, *11*, 3163−3168.
(39) Lee, K. H.; Schwenn, P. E.; Smith, A. R. G.; Cavaye, H.; Shaw, P. E.; James, M.; Krueger, K. B.; Gentle, I. R.; Meredith, P.; Burn, P. L. Morphology of All-Solution-Processed "Bilayer" Organic Solar Cells. *Adv. Mater.* **2011**, *23*, 766−770.
(40) Gevaerts, V. S.; Koster, L. J. A.; Wienk, M. M.; Janssen, R. A. J. Discriminating between Bilayer and Bulk Heterojunction Polymer:-Fullerene Solar Cells Using the External Quantum Efficiency. *ACS Appl. Mater. Interfaces* **2011**, *3*, 3252−3255.
(41) Rochester, C. W.; Mauger, S. A.; Moulé, A. J. Investigating the Morphology of Polymer/Fullerene Layers Coated Using Orthogonal Solvents. *J. Phys. Chem. C* **2012**, *116*, 7287−7292.
(42) Ayzner, A. L.; Doan, S. C.; Tremolet de Villers, B.; Schwartz, B. Ultrafast Studies of Exciton Migration and Polaron Formation in Sequentially Solution-Processed Conjugated Polymer/Fullerene Quasi-Bilayer Photovoltaics. *J. Phys. Chem. Lett.* **2012**, *3*, 2281−2287.
(43) Yang, B.; Yuan, Y.; Huang, J. Reduced Bimolecular Charge Recombination Loss in Thermally Annealed Bilayer Heterojunction Photovoltaic Devices with Large External Quantum Efficiency and Fill Factor. *J. Phys. Chem. C* **2014**, *118*, 5196−5202.
(44) Zhang, G.; Huber, R. C.; Ferreira, A. S.; Boyd, S. D.; Luscombe, C. K.; Tolbert, S. H.; Schwartz, B. J. Crystallinity Effects in Sequentially Processed and Blend-Cast Bulk-Heterojunction Polymer/Fullerene Photovoltaics. *J. Phys. Chem. C* **2014**, *118*, 18424−18435.
(45) Hawks, S. A.; Aguirre, J. C.; Schelhas, L. T.; Thompson, R. J.; Huber, R. C.; Ferreira, A. S.; Zhang, G.; Herzing, A. A.; Tolbert, S. H.; Schwartz, B. J. Comparing Matched Polymer:Fullerene Solar Cells Made by Solution-Sequential Processing and Traditional Blend Casting: Nanoscale Structure and Device Performance. *J. Phys. Chem. C* **2014**, *118*, 17413−17425.
(46) Clulow, A. J.; Tao, C.; Lee, K. H.; Velusamy, M.; McEwan, J. A.; Shaw, P. E.; Yamada, N. L.; James, M.; Burn, P. L.; Gentle, I. R.; Meredith, P. Time-Resolved Neutron Reflectometry and Photovoltaic Device Studies on Sequentially Deposited PCDTBT-Fullerene Layers. *Langmuir.* **2014**, *30*, 11474−11484.
(47) Chen, D.; Liu, F.; Wang, C.; Nakahara, A.; Russell, T. P. Bulk Heterojunction Photovoltaic Active Layers via Bilayer Interdiffusion. *Nano Lett.* **2011**, *11*, 2071−2078.
(48) Moon, J. S.; Takacs, C. J.; Sun, Y.; Heeger, A. J. Spontaneous Formation of Bulk Heterojunction Nanostructures: Multiple Routes to Equivalent Morphologies. *Nano Lett.* **2011**, *11*, 1036−1039.
(49) Treat, N. D.; Brady, M. A.; Smith, G.; Toney, M. F.; Kramer, E. J.; Hawker, C. J.; Chabinyc, M. L. Interdiffusion of PCBM and P3HT Reveals Miscibility in a Photovoltaically Active Blend. *Adv. Energy Mater.* **2011**, *1*, 82−89.
(50) Liu, F.; Gu, Y.; Wang, C.; Zhao, W.; Chen, D.; Briseno, A. L.; Russell, T. P. Efficient Polymer Solar Cells Based on A Low Bandgap Semi-Crystalline DPP Polymer-PCBM Blends. *Adv. Mater.* **2012**, *24*, 3947−3951.
(51) Ferdous, S.; Liu, F.; Wang, D.; Russell, T. P. Solvent-Polarity-Induced Active Layer Morphology Control in Crystalline Diketopyrrolopyrrole-Based Low Band Gap Polymer Photovoltaics. *Adv. Energy Mater.* **2014**, *4*, 1300834.
(52) Aapg BulletinLi, W.; Hendriks, K. H.; Roelofs, W. S. C.; Kim, Y.; Wienk, M. M.; Janssen, R. A. J. Efficient Small Bandgap Polymer Solar Cells with High Fill Factors for 300 nm Thick Films. *Adv. Mater.* **2013**, *25*, 3182−3186.
(53) Li, W.; Hendriks, K. H.; Furlan, A.; Roelofs, W. S.; Meskers, S. C.; Wienk, M. M.; Janssen, R. A. Effect of the Fibrillar Microstructure on the Efficiency of High Molecular Weight Diketopyrrolopyrrole-Based Polymer Solar Cells. *Adv. Mater.* **2014**, *26*, 1565−1570.
(54) Li, W.; Furlan, K. H. A.; Roelofs, W. S. C.; Wienk, M. M.; Janssen, R. A. J. Universal Correlation between Fibril Width and Quantum Efficiency in Diketopyrrolopyrrole-Based Polymer Solar Cells. *J. Am. Chem. Soc.* **2013**, *135*, 18942−18948.
(55) Li, W.; Furlan, A.; Hendriks, K. H.; Wienk, M. M.; Janssen, R. A. J. Efficient Tandem and Triple-Junction Polymer Solar Cells. *J. Am. Chem. Soc.* **2013**, *135*, 5529−5532.
(56) Hendriks, K. H.; Li, W.; Wienk, M. M.; Janssen, R. A. J. Small-Bandgap Semiconducting Polymers with High Near-Infrared Photoresponse. *J. Am. Chem. Soc.* **2014**, *136*, 12130−12136.
(57) Cheng, P.; Li, Y.; Zhan, X. A DMF-Assisted Solution Process Boosts the Efficiency in P3HT: PCBM Solar Cells up to 5.31%. *Nanotechnology* **2013**, *24*, 484008.